



# Lanthanide compounds as catalysts for the one-step synthesis of vinyl chloride from ethylene



Matthias Scharfe<sup>1</sup>, Pedro A. Lira-Parada<sup>1</sup>, Amol P. Amrute, Sharon Mitchell, Javier Pérez-Ramírez<sup>\*</sup>

Institute for Chemical and Bioengineering, Department of Chemistry and Applied Biosciences, ETH Zurich, Vladimir-Prelog-Weg 1, 8093 Zurich, Switzerland

## ARTICLE INFO

### Article history:

Received 28 July 2016

Revised 26 October 2016

Accepted 27 October 2016

### Keywords:

Ethylene oxychlorination

Lanthanides

Europium oxychloride

Vinyl chloride monomer

Bifunctional catalyst

Process intensification

## ABSTRACT

The industrial manufacture of vinyl chloride relies on a two-step process involving  $\text{CuCl}_2$ -catalyzed ethylene oxychlorination to ethylene dichloride followed by thermal cracking of the latter to vinyl chloride. This work evaluates a wide range of commercial and self-prepared lanthanide (La, Ce, Pr, Nd, Sm, Eu, Gd, Tb, Dy, Ho, and Er) compounds for the one-step production of vinyl chloride from ethylene in a fixed-bed reactor at 623–773 K and 1 bar using feed ratios of  $\text{C}_2\text{H}_4:\text{HCl}:\text{O}_2:\text{Ar}:\text{He} = 3\text{--}6:1\text{--}9.6:1\text{--}7.3:80\text{--}92$  and space times of 6–252  $\text{g h mol}^{-1}$  (based on ethylene). *Ex situ* characterization by X-ray diffraction, electron microscopy, and X-ray photoelectron spectroscopy reveals that the oxide forms of all compounds, except  $\text{CeO}_2$ , transform into their respective (oxy)chloride. Among all studied systems,  $\text{CeO}_2$  shows the highest activity but suffers from combustion forming  $\text{CO}_x$ , while europium oxychloride ( $\text{EuOCl}$ ) leads to the best vinyl chloride selectivity of 96% at 20%  $\text{C}_2\text{H}_4$  conversion for over 100 h on stream. Temperature-programmed reduction with  $\text{H}_2$ , temperature-programmed desorption of  $\text{NH}_3$ , and oxidation tests ( $\text{C}_2\text{H}_4$ ,  $\text{CO}$ , and  $\text{HCl}$  oxidation) unravel the unique balance of mild redox and enhanced acid properties of  $\text{EuOCl}$  compared to  $\text{CeO}_2$ , which suppress over-oxidation and boost ethylene dichloride dehydrochlorination. Strategies to couple the excellent selectivity of  $\text{EuOCl}$  with the high activity of  $\text{CeO}_2$  are demonstrated through the synthesis of homogeneous europium-cerium mixed oxides, combining two functions on a single surface. In addition, the engineering of a dual-bed reactor, integrating a  $\text{CeO}_2$  bed first to produce ethylene dichloride in high yield which is subsequently transformed to vinyl chloride over  $\text{EuOCl}$  leads to vinyl chloride yields of up to 30% per pass. These very promising findings constitute a crucial step for process intensification of polyvinyl chloride production and exploring the potential of rare-earth compounds in industrially-relevant reactions.

© 2016 Elsevier Inc. All rights reserved.

## 1. Introduction

Polyvinyl chloride (PVC, 44 Mton, annual global growth rate of 3.2%) is an integral part of modern society owing to its widespread applications that improve our everyday life [1,2]. Its monomer, chloroethene (commonly known as vinyl chloride and hereafter denoted as VCM), was first produced on a commercial scale in the 1920s through acetylene hydrochlorination over mercuric chloride catalysts, which still is the main production method in countries such as China, due to cheap availability of coal from which acetylene is produced [3,4]. However, the increasing demand for PVC and rising price of acetylene in the late 1950s prompted a shift in the feedstock to the more economical ethylene in the United States and Europe [3]. Since then, VCM is predomi-

nantly produced via a two-step process involving the selective oxychlorination of ethene (commonly known as ethylene) to 1,2-dichloroethane (commonly known as ethylene dichloride and hereafter denoted as EDC) over promoted  $\text{CuCl}_2/\gamma\text{-Al}_2\text{O}_3$  catalysts in fluidized-bed reactors ( $T = 473\text{--}573\text{ K}$ ,  $P = 10\text{ bar}$ ) and the subsequent thermal cracking of EDC to VCM ( $T = 773\text{--}873\text{ K}$ ,  $P = 25\text{--}35\text{ bar}$ ) [3–5]. The greatest limitations of the current process are the stability issues faced by the copper catalyst, and the limited per pass conversion (50–60% with VCM selectivity >98%) and high energy demand of the thermal cracking [3]. Despite continued efforts to optimize the robustness of the catalyst by doping with additives such as alkali (Li, Na, K), alkaline earth (Mg, Ca), and rare earth metals (La, Ce), the copper chloride phase is still prone to volatilization and particle agglomeration [6–10]. Besides, the possible intensification of VCM production by integration of the oxychlorination and dehydrochlorination reactions as a one-step process requires a novel catalyst which can combine two functions.

<sup>\*</sup> Corresponding author.

E-mail address: [jpr@chem.ethz.ch](mailto:jpr@chem.ethz.ch) (J. Pérez-Ramírez).

<sup>1</sup> Equal contribution.

In order to achieve this goal, new materials such as non-halide copper containing catalysts [11] and lanthanide (oxy)chlorides [12], particularly lanthanum oxychlorides, have been reported in the patent literature. However, none of these systems is realized on an industrial scale, most likely due to the low per pass VCM yields and/or stability hurdles faced by these catalysts. Recently, we have uncovered the high stability and remarkable yield of chlorinated compounds (25% VCM, 25% EDC) over  $\text{CeO}_2$ . This outstanding performance was attributed to the integration of both redox sites, which catalyze the ethylene oxychlorination to EDC, and acid sites, responsible for the dehydrochlorination of EDC to VCM, on the same catalyst surface.

In spite of these encouraging results,  $\text{CeO}_2$  offers significant margins for improvement. In particular, a considerable amount of over-chlorinated compounds (1,2-dichloroethene, commonly known as 1,2-dichloroethylene and hereafter denoted as 1,2-DCE) and combustion products ( $\text{CO}_x$ ) were also formed, decreasing the overall selectivity of EDC and VCM. Moreover, only moderate dehydrochlorination activity was observed. Thus, it can be anticipated that materials exhibiting milder oxidative properties and higher density of strong sites than ceria could lead to enhanced performance. Surprisingly, despite their extensive use as dopants of the  $\text{CuCl}_2/\gamma\text{-Al}_2\text{O}_3$  catalysts, lanthanide compounds were never systematically investigated as the main active phase for the conversion of ethylene to VCM. Besides, they were investigated in several other catalyst formulations mainly as dopants and supports [14–18], with the exception of cerium oxide and lanthanum oxide (or (oxy)chloride) which are also studied as the primary catalytic phase in oxidative processes, including CO oxidation [19,20], isobutane oxidation [21], HCl oxidation [22,23], methane oxidative coupling [24], selective reduction of nitrogen oxides [19,25], and methane oxychlorination [26,27].

Herein, the comparison of the performance of a broad set of the most abundant rare-earth compounds leads to the discovery of the exceptional performance of europium oxychloride, exhibiting 96% VCM selectivity at 20% conversion for over 100 h on stream. Structural, redox, and acidic properties are investigated to rationalize the superior performance of europium oxychloride with respect to other lanthanides and parametric studies give insight to the distribution of products. In order to attain superior VCM yields, this novel active phase is combined with the high activity of  $\text{CeO}_2$  by synthesis of mixed oxides and through dual-bed reactor concepts. This study comprises the first practically-relevant application of europium in heterogeneous catalysis and the materials presented here have great potential to be explored in challenging catalyzed reactions, particularly toward the functionalization of hydrocarbons.

## 2. Experimental methods

### 2.1. Catalyst preparation

Commercial  $\text{La}_2\text{O}_3$  (Alfa Aesar, 99.99%),  $\text{Pr}_2\text{O}_3$  (Alfa Aesar, 99.9%),  $\text{Nd}_2\text{O}_3$  (Sigma-Aldrich, 99.9%),  $\text{Sm}_2\text{O}_3$  (Sigma-Aldrich, 99.9%),  $\text{Eu}_2\text{O}_3$  (Sigma-Aldrich, 99.5%),  $\text{Gd}_2\text{O}_3$  (Alfa Aesar, 99.99%),  $\text{Tb}_2\text{O}_3$  (Strem Chemicals, 99.9%),  $\text{Dy}_2\text{O}_3$  (ABCR, 99.99%),  $\text{Ho}_2\text{O}_3$  (Fluka Chemie, 99.9%), and  $\text{Er}_2\text{O}_3$  (Fluka Chemie, 99.9%) were calcined at 773 K, and  $\text{CeO}_2$  (Sigma-Aldrich, 99.9%) at 773 K and 1173 K in static air using a heating rate of  $5\text{ K min}^{-1}$  and an isothermal step of 5 h prior to their use in catalytic studies. Analysis by X-ray diffraction revealed that the commercial praseodymium oxide actually consisted of  $\text{Pr}_4\text{O}_7$  and thus it is denoted as such hereafter. Europium oxide ( $\text{Eu}_2\text{O}_3\text{-p-}T_{\text{cal}}$ , where  $T_{\text{cal}}$  denotes the calcination temperature in K), cerium oxide ( $\text{CeO}_2\text{-p-}T_{\text{cal}}$ ), and mixed europium-cerium oxides ( $\text{Eu}_x\text{Ce}_{1-x}\text{O}_{2-0.5x}\text{-cp-}T_{\text{cal}}$ , where  $x$

represents the molar fraction of Eu in the range of 0.3–0.9) were synthesized by precipitation (p, single oxides) and coprecipitation (cp, mixed oxides) following a protocol reported elsewhere [13]. Briefly, the metal nitrates ( $\text{Eu}_2(\text{NO}_3)_3 \cdot 6\text{H}_2\text{O}$  (ABCR, 99.9%) for  $\text{Eu}_2\text{O}_3\text{-p}$ ,  $\text{Ce}(\text{NO}_3)_3 \cdot 6\text{H}_2\text{O}$  (ABCR, 99.9%) for  $\text{CeO}_2\text{-p}$ , or mixtures for  $\text{Eu}_x\text{Ce}_{1-x}\text{O}_{2-0.5x}\text{-cp}$ ) were dissolved in deionized water under stirring and  $\text{H}_2\text{O}_2$  (Acros Organics, 35%) was added to the solution to obtain a molar  $\text{H}_2\text{O}_2\text{:M}$  ratio of 3 ( $\text{M} = \text{Eu}, \text{Ce}, \text{or Eu} + \text{Ce}$ ). The coprecipitation was achieved by the dropwise addition of aqueous  $\text{NH}_4\text{OH}$  (Sigma-Aldrich, 30%) until a pH of 10.5 was reached. The slurry was stirred for 4 h and washed with deionized water. Upon filtration, the precipitate was dried at 393 K for 12 h and calcined at 773 K for  $\text{CeO}_2\text{-p}$ , 773–1173 K for  $\text{Eu}_2\text{O}_3\text{-p}$ , and 773 K for  $\text{Eu}_x\text{Ce}_{1-x}\text{O}_{2-0.5x}\text{-cp}$  in flowing air using a heating rate of  $5\text{ K min}^{-1}$  and an isothermal step of 5 h.

### 2.2. Characterization

The metal content was determined by X-ray fluorescence (XRF) spectroscopy using an Orbis PC Micro-EDXRF analyzer with a Rh source (15 kV, 500  $\mu\text{A}$ ) and a silicon drift detector. Powder X-ray diffraction (XRD) was measured using a PANalytical X'Pert PRO-MPD diffractometer and  $\text{Cu K}\alpha$  radiation ( $\lambda = 0.15418\text{ nm}$ ). The data were recorded in the  $10\text{--}70^\circ 2\theta$  range with an angular step size of  $0.017^\circ$  and a continuing time of 0.26 s per step.  $\text{N}_2$  sorption at 77 K was measured in a Quantachrome Quadrasorb-SI analyzer. Prior to the measurements, the samples were outgassed to 50 mbar at 573 K for 3 h. The Brunauer-Emmett-Teller (BET) method [28] was applied to calculate the total surface area,  $S_{\text{BET}}$ , in  $\text{m}^2\text{ g}^{-1}$ . High-resolution transmission electron microscopy (HRTEM) and elemental mapping using energy-dispersive X-ray spectroscopy (EDX) were conducted on a FEI Talos microscope operated at 200 kV. All samples were dispersed as dry powders onto lacey carbon coated nickel or molybdenum grids. X-ray photoelectron spectroscopy (XPS) measurements were performed on a Physical Electronics Quantum 2000 X-ray photoelectron spectrometer using monochromatic  $\text{Al K}\alpha$  radiation generated from an electron beam operated at 15 kV, and equipped with a hemispherical capacitor electron-energy analyzer. The powdered sample was firmly pressed onto the foil. The area analyzed was 150  $\mu\text{m}$  in diameter and the electron take-off angle was  $45^\circ$ . The pass energy used for the detailed spectra of the C 1s, O 1s, Cl 2p, Eu 3d, Eu 4d, and Ce 3d core levels was 46.95 eV to yield a total analyzer energy resolution of 0.95 eV. The spectrometer energy scale was calibrated for the Au 4f electrons to be at  $84.0 \pm 0.1\text{ eV}$ . Partial compensation of surface charging during spectra acquisition was obtained by the simultaneous operation of electron and argon ion neutralizers. Elemental concentrations are given in atomic percent using the measured photoelectron peak areas after Shirley background subtraction and the built-in sensitivity factors for calculation. Temperature-programmed desorption of ammonia ( $\text{NH}_3\text{-TPD}$ ) and temperature-programmed reduction with hydrogen ( $\text{H}_2\text{-TPR}$ ) were performed using a Micromeritics Autochem II 2920 unit equipped with a thermal conductivity detector coupled to a MKS Cirrus 2 mass spectrometer. The powder sample (0.1 g) was loaded into a U-shaped quartz micro-reactor, pretreated in He ( $20\text{ cm}^3\text{ STP min}^{-1}$ ) at 573 K for 3 h, and cooled to 373 K in He. For  $\text{NH}_3\text{-TPD}$  experiments, ammonia was chemisorbed at 473 K in three consecutive cycles of saturation with 5 vol.%  $\text{NH}_3/\text{He}$  ( $20\text{ cm}^3\text{ STP min}^{-1}$ ) for 30 min followed by purging with He ( $20\text{ cm}^3\text{ STP min}^{-1}$ ) at the same temperature for 30 min. Desorption of  $\text{NH}_3$  was monitored in the range of 473–1273 K using a heating rate of  $20\text{ K min}^{-1}$  and a He flow of  $20\text{ cm}^3\text{ STP min}^{-1}$ . For  $\text{H}_2\text{-TPR}$  experiments, the sample was pretreated in He ( $20\text{ cm}^3\text{ STP min}^{-1}$ ) at 423 K for 1 h, and cooled to room

temperature followed by ramping the temperature at  $10\text{ K min}^{-1}$  up to  $1273\text{ K}$  in  $5\text{ vol.}\% \text{ H}_2$  ( $20\text{ cm}^3\text{ STP min}^{-1}$ ).

### 2.3. Catalytic tests

The gas-phase oxychlorination of ethylene was investigated at ambient pressure in a continuous-flow fixed-bed reactor (Scheme 1). The set-up consists of (i) mass flow controllers to feed  $\text{C}_2\text{H}_4$  (PanGas, 20.15% in He), HCl (Air Liquide, purity 2.8, anhydrous),  $\text{O}_2$  (Messer, 10.06% in He), He (PanGas, purity 5.0) as a carrier gas, and Ar (PanGas, purity 5.0) as an internal standard, (ii) a syringe pump (Nexus 6000, Chemyx) to feed EDC (Fluka, 99.5%), (iii) a vaporizer operated at  $403\text{ K}$  accommodating a quartz T-connector filled with glass beads to vaporize EDC, (iv) an electrically heated oven hosting a quartz micro-reactor equipped with a K-type thermocouple whose tip reaches the center of the catalyst bed, (v) downstream heat tracing to avoid any condensation of the reactants and products, and (vi) a gas chromatograph coupled to a mass spectrometer (GC-MS) for on-line analysis. The effluent stream was neutralized by passing it through an impinging bottle containing an aqueous NaOH solution ( $1\text{ M}$ ). The catalyst ( $W_{\text{cat}} = 0.05\text{--}2\text{ g}$ , particle size,  $d_p = 0.4\text{--}0.6\text{ mm}$ ) was loaded in the micro-reactor ( $10\text{ mm}$  inner diameter) and pretreated in He at  $473\text{ K}$  for  $30\text{ min}$ . Thereafter, a total flow ( $F_T$ ) of  $100\text{ cm}^3\text{ STP min}^{-1}$  containing  $3\text{--}6\text{ vol.}\% \text{ C}_2\text{H}_4$ ,  $1\text{--}9.6\text{ vol.}\% \text{ HCl}$ ,  $1\text{--}7\text{ vol.}\% \text{ O}_2$ , and  $3\text{ vol.}\% \text{ Ar}$  as internal standard, balanced in He was fed to the reactor at a bed temperature ( $T$ ) of  $623\text{--}773\text{ K}$  and pressure ( $P$ ) of  $1\text{ bar}$ . Note that relatively low feed concentrations were selected to prevent corrosion, enable safe handling, and minimize the formation of hot spots in the catalyst bed due to the high reaction exothermicity. Temperature measurements in a reference experiment on  $\text{CeO}_2\text{--}1173$  (at  $31\% \text{ C}_2\text{H}_4$  conversion), evidenced a temperature gradient of  $0.9\text{ K}$  across the bed when the temperature in the center of the catalyst bed was set to  $673\text{ K}$  (Scheme 1). The standard conditions of  $3\text{ vol.}\% \text{ C}_2\text{H}_4$ ,  $4.8\text{ vol.}\% \text{ HCl}$ , and  $3\text{ vol.}\% \text{ O}_2$  were chosen based on the literature [8,13]. The space time, defined as the ratio of the catalyst mass and the inlet molar flow of ethylene as the limiting reactant,  $W_{\text{cat}}/\dot{n}^0(\text{C}_2\text{H}_4)$ , was varied in the range of  $6\text{--}252\text{ g h mol}^{-1}$ . In the dehydrochlorination tests,  $1.5\text{ vol.}\% \text{ EDC}$  was fed to the catalyst ( $W_{\text{cat}} = 0.5\text{ g}$ ,  $d_p = 0.4\text{--}0.6\text{ mm}$ ) using He as carrier gas ( $F_T = 100\text{ cm}^3\text{ STP min}^{-1}$ ) with or without addition of HCl ( $4.8\text{ vol.}\%$ ) and  $\text{O}_2$  ( $3\text{ vol.}\%$ ) at  $T = 523\text{--}773\text{ K}$  and  $W_{\text{cat}}/\dot{n}^0(\text{EDC}) = 126\text{ g h mol}^{-1}$ . Prior to the analysis of the reaction mixtures, the catalysts were equilibrated for at least  $1\text{ h}$  under each condition. The gas composition at the reactor outlet containing reactants ( $\text{C}_2\text{H}_4$ ,  $\text{O}_2$ , HCl) and products (EDC, VCM, 1,2-DCE, CO,  $\text{CO}_2$ ) was analyzed online using a gas chromatograph equipped with a GS-CarbonPLOT column coupled to a mass spectrometer (Agilent GC 7890B, Agilent MSD 5977A) with a triple-axis detector and an electron multiplier. A representative chromatogram is depicted as an inset in Scheme 1. In the oxidation tests,  $\text{C}_2\text{H}_4$  ( $3\text{ vol.}\%$ ), CO ( $2.5\text{ vol.}\%$ ), or HCl ( $3\text{ vol.}\%$ ) and  $\text{O}_2$  were fed in a 1:1 volumetric ratio. In the HCl oxidation tests, the  $\text{Cl}_2$  production was quantified by offline iodometric titration (using a Mettler Toledo G20 Compact Titrator) of triiodide, formed by purging the  $\text{Cl}_2$  containing reactor outlet through an aqueous KI (Sigma-Aldrich, 99.5%) solution ( $0.1\text{ M}$ ), with  $0.01\text{ M}$  sodium thiosulfate solution (Sigma-Aldrich, 99.99%). The conversion of HCl,  $X(\text{HCl})$ , was calculated using Eq. (1),

$$X(\text{HCl}) = \frac{2x_{\text{Cl}_2,\text{outlet}}}{x_{\text{HCl},\text{inlet}}} \cdot 100, \% \quad (1)$$

where  $x_{\text{HCl},\text{inlet}}$  and  $x_{\text{Cl}_2,\text{outlet}}$  denote the volumetric concentration of HCl and  $\text{Cl}_2$  at the reactor inlet and outlet, respectively. The conver-

sion of carbon containing reactant,  $X(i)$ , where  $i$  denotes  $\text{C}_2\text{H}_4$  or CO, was calculated according to Eq. (2),

$$X(i) = \frac{x_{i,\text{inlet}} - x_{i,\text{outlet}}}{x_{i,\text{inlet}}} \cdot 100, \% \quad (2)$$

where  $x_{i,\text{inlet}}$  and  $x_{i,\text{outlet}}$  denote the volumetric concentration of  $i$  at the reactor inlet and outlet, respectively. The selectivity and yield of a reaction product  $j$ ,  $S(j)$  and  $Y(j)$ , were calculated according to Eqs. (3) and (4),

$$S(j) = \frac{x_j/v_j}{\sum x_j/v_j} \cdot 100, \% \quad (3)$$

$$Y(j) = \frac{x(i)S(j)}{100}, \% \quad (4)$$

where  $x_j$  and  $v_j$  denote the volumetric concentrations of product  $j$  at the reactor outlet and the corresponding stoichiometric factor with respect to the number of carbon atoms, respectively (e.g.,  $\text{C}_2\text{H}_4 + 2\text{O}_2 \rightarrow 2\text{CO} + 2\text{H}_2\text{O}$ ,  $v_{\text{CO}} = 2$ ). The rate of VCM production,  $r(\text{VCM})$ , and the rate of ethylene consumption,  $r(\text{C}_2\text{H}_4)$  were calculated using Eqs. (5) and (6):

$$r(\text{VCM}) = \frac{x_{\text{C}_2\text{H}_4,\text{inlet}} \cdot F_T \cdot X(\text{C}_2\text{H}_4)/100 \cdot P \cdot S(\text{VCM})/100}{R \cdot T_{\text{STP}} \cdot W_{\text{cat}} \cdot S_{\text{BET}}}, \text{ mol h}^{-1} \text{ m}^{-2} \quad (5)$$

$$r(\text{C}_2\text{H}_4) = \frac{x_{\text{C}_2\text{H}_4,\text{inlet}} \cdot F_T \cdot X(\text{C}_2\text{H}_4)/100 \cdot P}{R \cdot T_{\text{STP}} \cdot W_{\text{cat}} \cdot S_{\text{BET}}}, \text{ mol h}^{-1} \text{ m}^{-2} \quad (6)$$

where  $x_{\text{C}_2\text{H}_4,\text{inlet}}$ ,  $R$ , and  $T_{\text{STP}}$ , denote volumetric reactor inlet  $\text{C}_2\text{H}_4$  concentration, gas constant, and temperature at standard conditions, catalyst mass, and specific surface area, respectively. The carbon mass balance error  $\varepsilon_c$  was determined using Eq. (7):

$$\varepsilon_c = \left| \frac{\sum x_{i,j,\text{inlet}} - v_{i,j,\text{inlet}} - \sum x_{i,j,\text{outlet}}/v_{i,j,\text{outlet}}}{\sum x_{i,j,\text{inlet}}/v_{i,j,\text{inlet}}} \right| \cdot 100, \% \quad (7)$$

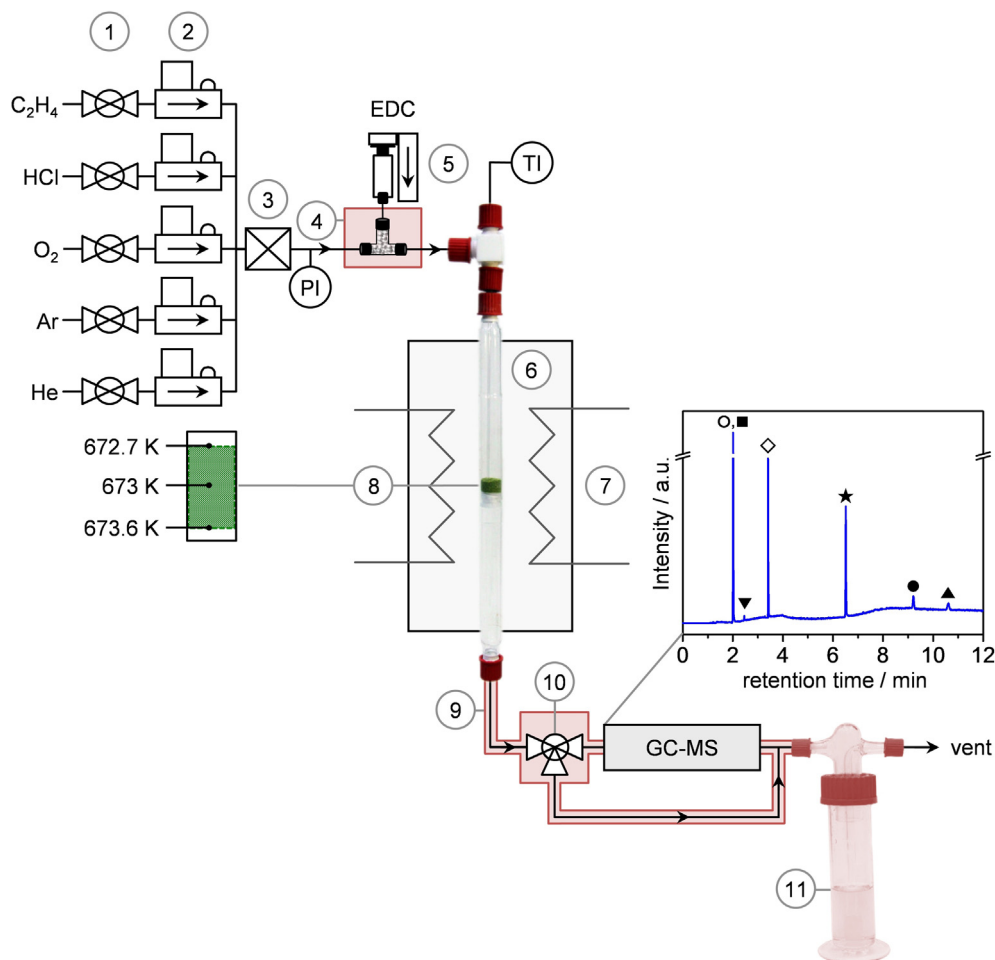
where  $x_{i,j}$  and  $v_{i,j}$  denote the concentration of reactant  $i$  or product  $j$  at the reactor inlet or outlet and the corresponding stoichiometric factor with respect to the number of carbon atoms, respectively. Each catalytic data point reported is an average of at least three measurements. The carbon mass balance in all catalytic tests closed at  $96\%$  or higher. After the tests, the catalyst bed was quenched to room temperature in He flow.

## 3. Results and discussion

### 3.1. Performance of lanthanide compounds in ethylene oxychlorination

The lanthanide oxides evaluated in this study were characterized by XRF (Fig. S1) and XRD (Fig. S2) to confirm their compositional and phase purity. All results coincided with the manufacturers specifications except in the case of praseodymium, which was found to be present mainly in the form of  $\text{Pr}_4\text{O}_7$  rather than  $\text{Pr}_2\text{O}_3$ . Besides, the post-reaction structural analysis revealed that all samples except  $\text{CeO}_2$  undergo phase transitions to their respective (oxy)chloride phase (*vide infra*; e.g.,  $\text{Eu}_2\text{O}_3$  transforms to  $\text{EuOCl}$ ). For this reason, the catalysts are denoted according to the crystalline phase evidenced by XRD in the equilibrated materials (after treatment for at least  $1\text{ h}$  under reaction conditions).

Comparative assessment in ethylene oxychlorination (Fig. 1), revealed that the rare earth materials can be classified into three groups according to their performance. The first ( $\text{SmOCl}$ ,  $\text{ErCl}_3$ ,  $\text{TbOCl}$ , and  $\text{HoOCl}$ ) and second ( $\text{PrOCl}$ ,  $\text{DyOCl}$ ,  $\text{GdOCl}$ ,  $\text{NdCl}_3$ ,  $\text{LaCl}_3$ ) both display only minor activity, and are differentiated by the observation of chlorinated products (EDC or VCM) which are only formed over the latter group. In contrast, the third group, compris-



**Scheme 1.** Scheme of the laboratory set-up used for the catalytic studies. 1: on-off valves, 2: mass flow controllers, 3: mixer, 4: vaporizer, 5: syringe pump, 6: quartz reactor, 7: oven, 8: catalyst bed, 9: heat tracing, 10: three-way bypass valve, 11: NaOH scrubber, PI: pressure indicator, and TI: temperature indicator. The three positions at which the temperature was measured in the catalyst bed are indicated on the left, lying within  $\pm 1$  K (measured in a reference experiment over  $\text{CeO}_2$ -1173 at 31%  $\text{C}_2\text{H}_4$  conversion). The inset on the right depicts a representative chromatogram where the peaks are assigned to the following compounds:  $\diamond$ ,  $\text{C}_2\text{H}_4$ ;  $\blacktriangledown$ ,  $\text{CO}_2$ ;  $\star$ , vinyl chloride;  $\bullet$ , 1,2-cis-dichloroethene, and  $\blacktriangle$ , ethylene dichloride.

ing  $\text{CeO}_2$  and  $\text{EuOCl}$ , stands out, exhibiting notably higher  $\text{C}_2\text{H}_4$  conversion and selectivity to chlorinated products than either of the other groups.  $\text{CeO}_2$ , which was previously studied in this reaction, demonstrated the highest yield of chlorinated compounds. On the other hand,  $\text{EuOCl}$  interestingly showed the highest selectivity to VCM (51% versus 30% over  $\text{CeO}_2$  at 12% and 26%  $\text{C}_2\text{H}_4$  conversion, respectively) and no formation of  $\text{CO}_2$ . Two advantageous features of  $\text{EuOCl}$  can be highlighted: the suppressed  $\text{CO}_2$  formation indicates an inherently lower reducibility of  $\text{EuOCl}$  with respect to  $\text{CeO}_2$  while still maintaining the ability to form EDC and the low EDC selectivity over  $\text{EuOCl}$  evidences that more than 90% of the EDC formed is directly transformed to VCM. In addition,  $\text{EuOCl}$  shows a 1.5-fold higher relative ethylene conversion per unit surface area of the equilibrated sample as determined by  $\text{N}_2$  sorption (Table 1) than  $\text{CeO}_2$ . In fact, comparison of the surface normalized rate of VCM production as a function of the inverse of temperature (Fig. 1, inset) reveals that  $\text{EuOCl}$  outperforms  $\text{CeO}_2$  in the whole temperature range.

Previously [13], we showed that the ethylene oxychlorination performance of  $\text{CeO}_2$  could be enhanced through the preparation of materials with higher surface areas by precipitation. Following this strategy, a series of europium-based catalysts ( $\text{EuOCl}$ -p- $T_{\text{cal}}$ , where  $T_{\text{cal}}$  denotes the calcination temperature) were prepared with surface areas comparable to that of  $\text{CeO}_2$ . Surprisingly, how-

ever, these samples did not lead to the expected increase in conversion, but completely suppressed the oxidation reaction to  $\text{CO}$  and largely increased the yields of EDC and VCM (Fig. 1), which were highest over  $\text{EuOCl}$ -p-973. In this case,  $\text{EuOCl}$ -p-973 was found to be one order of magnitude more reactive than  $\text{CeO}_2$  and comparable to  $\text{EuOCl}$  in terms of surface normalized rate (Fig. 1, inset).

### 3.2. Catalyst evolution in ethylene oxychlorination

Analysis of the structure, composition, porosity, and surface properties of the equilibrated catalysts provides insight into the trends observed during the comparative evaluation in ethylene oxychlorination. As mentioned (*vide supra*), phase transformations were observed in all of the catalysts after evaluation in the ethylene oxychlorination reaction, except  $\text{CeO}_2$ . Nonetheless, this phase evolution should be regarded as an equilibration step leading to the successful formation of the active (oxy)chloride phase rather than proof of instability. In fact, no catalyst volatilization was evidenced. Comparison by XRD (Figs. 2 and S2) identifies three different degrees of transformation, encompassing the preservation of the bulk oxide ( $\text{CeO}_2$ ) [13,22], the formation of an oxychloride ( $\text{SmOCl}$ ,  $\text{TbOCl}$ ,  $\text{HoOCl}$ ,  $\text{PrOCl}$ ,  $\text{EuOCl}$ ), and the complete transformation to the chloride phase ( $\text{ErCl}_3$ ,  $\text{NdCl}_3$ ,  $\text{LaCl}_3$ ). Despite

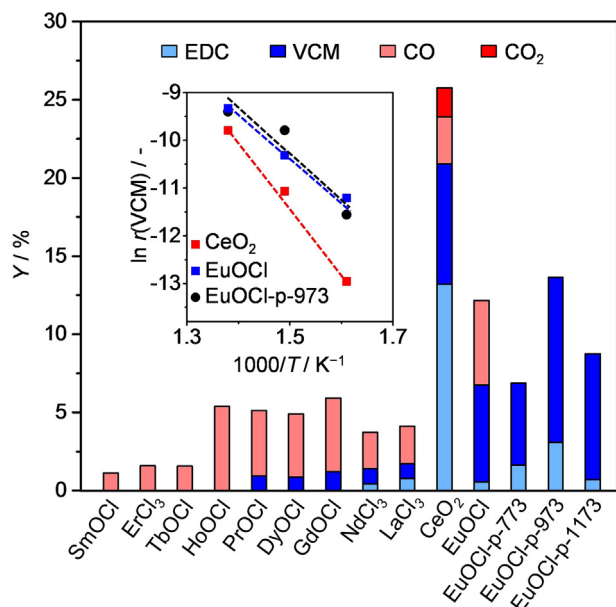


**Fig. 1.** Product yields (Y) in ethylene oxychlorination over single metal lanthanide catalysts. The inset depicts the Arrhenius plot of VCM formation over CeO<sub>2</sub>, EuOCl, and EuOCl-p-973. Conditions:  $T = 723$  K,  $\text{C}_2\text{H}_4:\text{HCl}:\text{O}_2:\text{Ar}:\text{He} = 3:4.8:3:3:86.2$ ,  $W_{\text{cat}}/\dot{n}^0(\text{C}_2\text{H}_4) = 63$  g h mol<sup>-1</sup>.

**Table 1**

Total surface area of the samples prior to (fresh) and after (equilibrated) ethylene oxychlorination. The nomenclature of the used samples reflects the main crystallographic phase identified in the catalyst.

Fresh sample <sup>a</sup>	$S_{\text{BET}}^b$ (m <sup>2</sup> g <sup>-1</sup> )	Equilibrated sample	$S_{\text{BET}}^b$ (m <sup>2</sup> g <sup>-1</sup> )
La <sub>2</sub> O <sub>3</sub>	6	LaCl <sub>3</sub>	8
CeO <sub>2</sub>	45	CeO <sub>2</sub>	28
Pr <sub>4</sub> O <sub>7</sub>	5	PrOCl	6
Nd <sub>2</sub> O <sub>3</sub>	32	NdCl <sub>3</sub>	21
Sm <sub>2</sub> O <sub>3</sub>	10	SmOCl	8
Eu <sub>2</sub> O <sub>3</sub>	11	EuOCl	8
Eu <sub>2</sub> O <sub>3</sub> -p-773	37	EuOCl-p-773	26
Eu <sub>2</sub> O <sub>3</sub> -p-973	31	EuOCl-p-973	23
Eu <sub>2</sub> O <sub>3</sub> -p-1173	14	EuOCl-p-1173	12
Gd <sub>2</sub> O <sub>3</sub>	5	GdOCl	16
Tb <sub>2</sub> O <sub>3</sub>	4	TbOCl	7
Dy <sub>2</sub> O <sub>3</sub>	29	DyOCl	25
Ho <sub>2</sub> O <sub>3</sub>	7	HoOCl	6
Er <sub>2</sub> O <sub>3</sub>	60	ErCl <sub>3</sub>	15

<sup>a</sup> All samples were commercial, except Eu<sub>2</sub>O<sub>3</sub>-p-*T*<sub>cat</sub>, which was obtained by precipitation and calcination at *T*<sub>cat</sub> K.

<sup>b</sup> BET method.

exhibiting distinct performance, only a single europium oxychloride phase is observed in EuOCl-p-973 and EuOCl. Slightly sharper reflections in the latter reflect increased average particle size, which is in line with lower surface area. A Scherrer-based analysis confirms an average crystal size of 31 nm for EuOCl in comparison with 13 nm for the EuOCl-p-973 sample.

Examination of LaCl<sub>3</sub>, EuOCl, and CeO<sub>2</sub> by TEM and elemental mapping clearly revealed the different extent of chlorination in these samples. LaCl<sub>3</sub> (Fig. 3a), which fully chlorinates upon equilibration under ethylene oxychlorination conditions, comprises large agglomerates of between 100 and 200 nm diameter. The relative intensity of the Cl and La lines in the EDX spectrum of ca. 3 agrees well with the stoichiometry of the metal chloride. Comparatively, EuOCl as well as EuOCl-p-973 (Fig. 3b and c) features much smaller particles of ca. 40 nm in diameter and a Cl:Eu intensity ratio close to unity, as expected from a pure oxychloride phase. In both cases, no considerable change in crystal size is observed

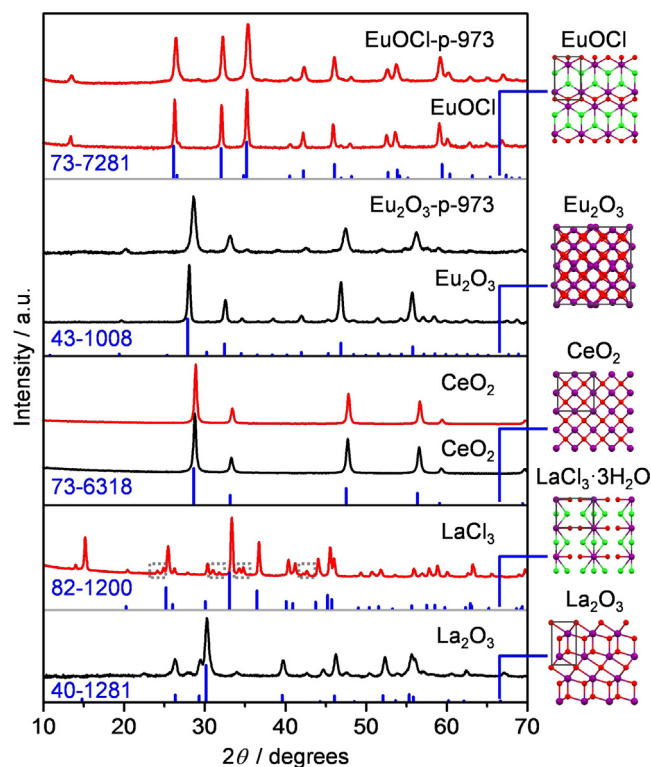


**Fig. 2.** XRD patterns of selected catalysts prior to (black) and after (red) ethylene oxychlorination. Vertical lines beneath the diffractograms and structures on the right denote identified crystalline phases according to the ICDD PDF numbers provided on the left of the figure. The gray rectangles in the structures represent the corresponding unit cells. Dashed boxes in the diffractogram of LaCl<sub>3</sub> highlight the reflections for LaOCl·H<sub>2</sub>O (ICDD PDF 70-2139). XRD analysis of all other investigated lanthanide-based catalysts is depicted in Fig. S2. (For interpretation of the references to colour in this figure legend, the reader is referred to the web version of this article.)

between the as prepared and equilibrated materials. Finally, CeO<sub>2</sub> evidences even smaller nanoparticles of 10–20 nm (as prepared: 5–10 nm) in diameter and exhibits only a minor chlorine peak in the EDX spectrum (Fig. 3d, inset), consistent with the low intensity of this element in the corresponding map and the preservation of the oxide phase evidenced by XRD. To detect possible differences in the surface and bulk composition, XPS analysis was conducted for the as-prepared Eu<sub>2</sub>O<sub>3</sub>-p-973, which evidences a Eu 4d core level band structure composed of the Eu 4d<sub>3/2</sub> and Eu 4d<sub>5/2</sub> peaks, characteristic of Eu<sub>2</sub>O<sub>3</sub> (Fig. 4a) [29,30]. Upon use in ethylene oxychlorination, both of these peaks were shifted to higher binding energy by 2 eV, pointing to the presence of neighboring atoms of high electronegativity [29]. A signal detected in the survey spectrum at 198.5 eV [31] in the Cl 2p region unequivocally confirmed the presence of chlorine at the surface (Fig. 4b). In fact, the surface atomic concentrations of Eu, O, and Cl were determined to be 33%, 36%, and 30%, respectively, which is close to the stoichiometry of the oxychloride phase.

Overall, these results demonstrate that ethylene oxychlorination over the lanthanide compounds studied is essentially catalyzed by the oxychloride or chloride phase, including in the case of CeO<sub>2</sub> in which chloride species exist at the surface. However, there are no detectable structural differences between EuOCl and EuOCl-p-973 that would explain their disparity in selectivity. As on CeO<sub>2</sub> the suppression of combustion and the formation of VCM were linked to moderated oxidative properties (catalyzing ethylene oxychlorination to EDC) and the presence of acid sites (needed for EDC dehydrochlorination to VCM [32]), the properties

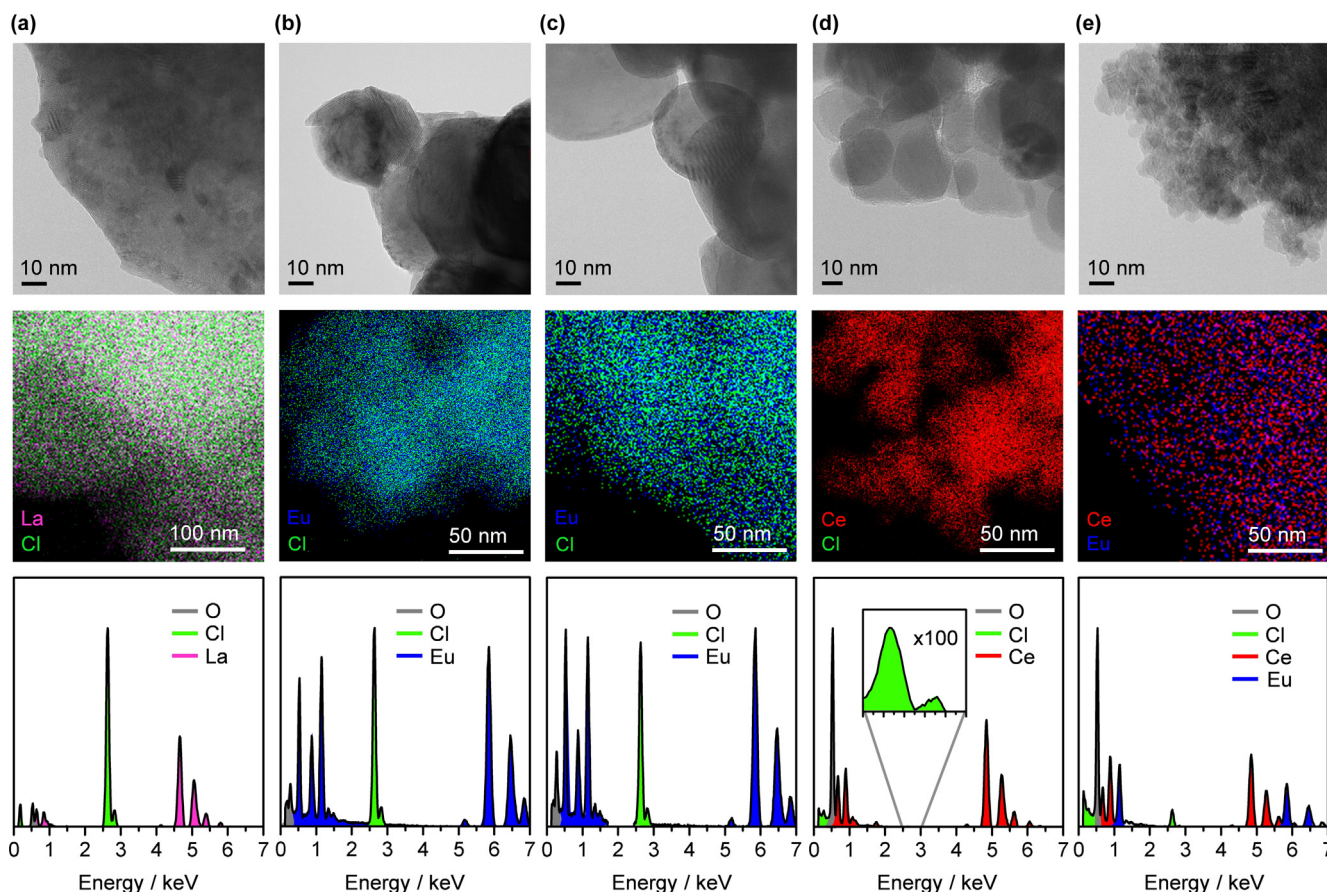


**Fig. 3.** HRTEM images (top), elemental maps (middle), and corresponding EDX spectra (bottom) of equilibrated catalysts: column (a) LaOCl, column (b) EuOCl, column (c) EuOCl-p-973, column (d) CeO<sub>2</sub>, and column (e) Eu<sub>0.4</sub>Ce<sub>0.6</sub>O<sub>1.8</sub>-cp-773.

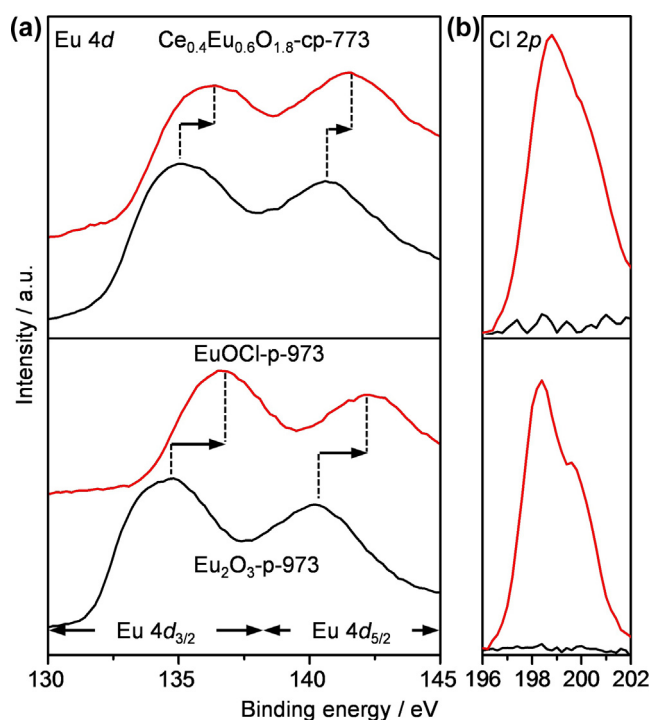


**Fig. 4.** (a) Eu 4d and (b) Cl 2p core level XPS spectra of fresh (black) and equilibrated (red) europium-based catalysts. (For interpretation of the references to colour in this figure legend, the reader is referred to the web version of this article.)

of EuOCl-p-973 and CeO<sub>2</sub> were investigated by H<sub>2</sub>-TPR and NH<sub>3</sub>-TPD. PrOCl was also studied as a moderately active and unselective reference.

The H<sub>2</sub>-TPR profile of CeO<sub>2</sub> (Fig. 5a) shows two H<sub>2</sub> consumption peaks at 761 and 1090 K, which are attributed to the reduction of labile surface or near-surface oxygen species and the bulk, respectively [33,34]. This very much resembles the analysis of the as-prepared CeO<sub>2</sub> samples [22] and indicates that the reducibility of this oxide is not significantly altered under reaction conditions. Pr<sub>4</sub>O<sub>7</sub> displays a H<sub>2</sub> consumption peak centered at 978 K, however, no H<sub>2</sub> consumption is observed for its analogue PrOCl, indicating that the oxychloride is irreducible in this temperature range. This explains the negligible yields of VCM and CO, observed over this catalyst, which are comparable to the inactive materials. Eu<sub>2</sub>O<sub>3</sub>-p-973 evidences a broad H<sub>2</sub> consumption peak in the range of 882–1197 K, while EuOCl-p-973 shows H<sub>2</sub> consumption at significantly higher temperature (similar trend for Eu<sub>2</sub>O<sub>3</sub> and EuOCl). Thus, the diminished reducibility of europium oxychlorides compared to CeO<sub>2</sub> is responsible for the lower activity and most importantly the suppression of combustion. However, it is still sufficient to catalyze the formation of EDC.

NH<sub>3</sub>-TPD analyses confirmed that the equilibrated CeO<sub>2</sub> and EuOCl-p-973 catalysts both exhibit significant NH<sub>3</sub> desorption in the range of 525–775 K (Fig. 5b), evidencing the presence of acid sites. This is in line with previous studies on CeO<sub>2</sub> after treatment under chlorination conditions [13,35]. The lower acidity of EuOCl with respect to EuOCl-p-973 is also in accordance with the lower VCM selectivity of the former. Surprisingly, PrOCl shows the highest amount of acid sites by far, which causes the complete transformation of any EDC produced to VCM. Quantification of the amount

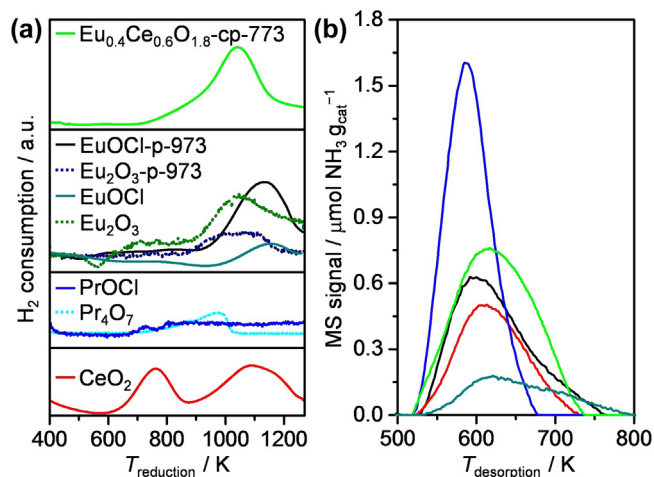


**Fig. 5.** (a) H<sub>2</sub>-TPR and (b) NH<sub>3</sub>-TPD profiles of selected fresh (dashed lines) and equilibrated (solid lines) catalysts.

of ammonia evolved from the two materials with highest VCM yields reveals a significantly higher acid site density in EuOCl-p-973 (1.92 μmol g<sup>-1</sup>) than CeO<sub>2</sub> (1.45 μmol g<sup>-1</sup>), explaining the enhanced VCM formation over the former.

### 3.3. Influence of operating conditions

In view of the unprecedented selectivity of EuOCl-p-973, the impact of reaction conditions (namely temperature, HCl and O<sub>2</sub> feed contents, and contact time) on the conversion and product distribution was studied (Fig. 6). These results are compared with CeO<sub>2</sub> calcined at 1173 K (CeO<sub>2</sub>-1173), which was previously reported in ethylene oxychlorination [13]. Both catalysts exhibit an increased conversion with temperature (Fig. 6a), but the enhancement is lower over EuOCl-p-973 than CeO<sub>2</sub>-1173. Accordingly, the apparent activation energy (determined from Arrhenius plots, Fig. S3) is slightly higher for CeO<sub>2</sub>-1173 (28 kJ mol<sup>-1</sup>) than for EuOCl-p-973 (17 kJ mol<sup>-1</sup>). Considering the product distribution, the selectivity to VCM increases with reaction temperature over both catalysts, which correlates with a parallel decrease in the EDC selectivity. No CO<sub>x</sub> formation is evidenced over EuOCl-p-973 up to 773 K at which point a minor amount of CO is observed, whereas CeO<sub>2</sub>-1173 suffers from over-oxidation above 673 K, leading to ca. 50% selectivity to CO<sub>x</sub> (at 50% C<sub>2</sub>H<sub>4</sub> conversion) at 773 K. However, in this comparison of the effect of temperature on the selectivity patterns of the catalysts, the conversion levels differ due to the stronger activity dependence on temperature of CeO<sub>2</sub> than that of EuOCl. Therefore, to decouple the effect of temperature and conversion, the latter was raised by changing the space time at 723 K over both catalysts (Fig. 6d). Upon increasing the C<sub>2</sub>H<sub>4</sub> conversion over EuOCl-p-973, the selectivity to VCM strongly increases and, reaching 100% at 25% conversion. The selectivity to EDC decreases in equal order, which is consistent with the successive transformation of ethylene to EDC and its dehydrochlorination to VCM. A qualitatively similar decrease of EDC selectivity is also observed over CeO<sub>2</sub>-1173 at comparable conversion levels. Nonetheless, the formation of combustion (CO<sub>x</sub>) and over-chlorinated (1,2-DCE) products is enhanced instead of VCM.

Varying the feed composition also highlights significant differences in the behavior of the two catalysts. Neither the conversion nor the product distribution is significantly affected by the HCl or O<sub>2</sub> feed contents within the investigated range (i.e., zero order with respect to HCl and O<sub>2</sub>) over EuOCl-p-973. In contrast,

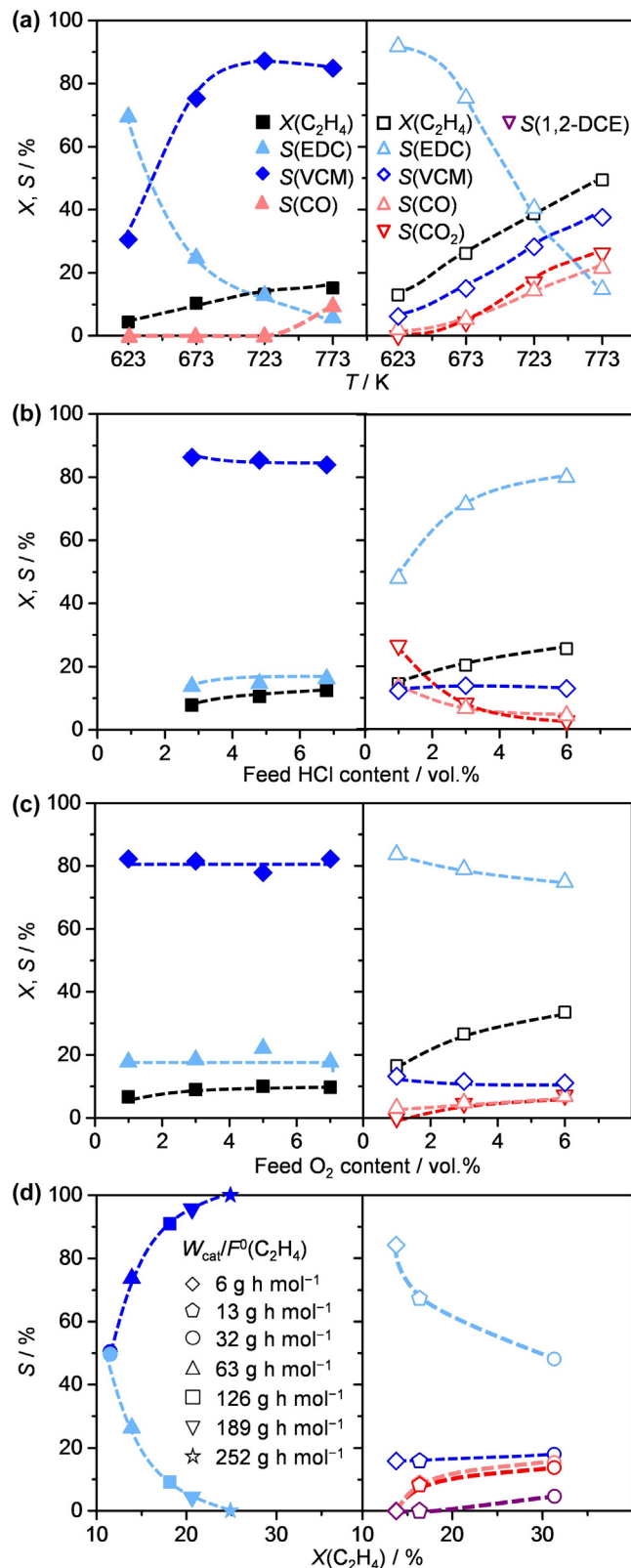


**Fig. 6.** C<sub>2</sub>H<sub>4</sub> conversion and product selectivity over EuOCl-p-973 (left) and CeO<sub>2</sub>-1173 (right) as a function of (a) T at fixed HCl (4.8 vol.%) and O<sub>2</sub> (3 vol.%) concentrations, (b) feed HCl content at fixed O<sub>2</sub> content (3 vol.%) at 723 K (EuOCl) and 673 K (CeO<sub>2</sub>), and (c) feed O<sub>2</sub> content at fixed HCl content (4.8 vol.%) at 723 K (EuOCl) and 673 K (CeO<sub>2</sub>). (d) Selectivity to products versus conversion at different space times at 723 K at fixed HCl (4.8 vol.%) and O<sub>2</sub> (3 vol.%) concentrations, color code as in a–c. Conditions: (a–c)  $W_{\text{cat}}/\dot{n}^0(\text{C}_2\text{H}_4) = 63 \text{ g h mol}^{-1}$ , (d)  $W_{\text{cat}}/\dot{n}^0(\text{C}_2\text{H}_4) = 6\text{--}252 \text{ g h mol}^{-1}$ .

CeO<sub>2</sub>-1173 exhibits a positive linear activity trend with the HCl feed content and a second order dependency with respect to oxygen (Fig. 6b and c). Furthermore, the EDC selectivity increases with the HCl content in the feed over CeO<sub>2</sub>-1173, compensated by decreased CO<sub>x</sub> formation. This is expected as a higher degree of chlorination lowers the oxidative strength of the CeO<sub>2</sub>-1173 surface [13,22] and provides more available sites for chlorination. The inverse argument applies for raising the oxygen content, which favors combustion and lowers the selectivity to EDC linearly by decreasing the degree of surface chlorination [22]. Combining these results with the insights gained from the bulk and surface characterization, important differences between the two materials can be pointed out. Although CeO<sub>2</sub>-1173 preserves the bulk structure of the oxide, the reaction environment alters the nature of the surface from a more oxide- to a more chloride-dominated structure, which have different oxidative properties. In contrast, once formed the surface structure of EuOCl-p-973 remains unaltered by the feed conditions. Thus, a change in reaction atmosphere only affects the thermodynamic equilibria, but not the nature of redox sites.

To further understand the selectivity patterns of catalysts in ethylene oxychlorination, the reaction was split into the four possible processes that can impact the VCM formation. These include the oxidation of C<sub>2</sub>H<sub>4</sub> to CO<sub>x</sub>, CO to CO<sub>2</sub>, and HCl to Cl<sub>2</sub>, as well as the dehydrochlorination of EDC to VCM (Fig. 7). Each reaction was performed over equilibrated samples: CeO<sub>2</sub> (exhibiting the highest activity), EuOCl-p-973 (attaining the highest VCM yield), and PrOCl (representative of samples exhibiting low activity and high CO formation). In C<sub>2</sub>H<sub>4</sub> and HCl oxidation reactions, CeO<sub>2</sub> is the most active material, especially at higher temperatures (Fig. 7a and b), which correlates with its higher reducibility (*vide supra*, Fig. 5a). PrOCl also shows activity for the oxidation of C<sub>2</sub>H<sub>4</sub> and CO, with similar or lower light-off temperatures compared to CeO<sub>2</sub>, respectively. Note that no CO<sub>2</sub> was generated on PrOCl during ethylene oxychlorination, while in separate oxidation experiments it converted both C<sub>2</sub>H<sub>4</sub> and CO to CO<sub>2</sub>. XRD analysis revealed that the PrOCl phase partially decomposes and re-transforms to the Pr<sub>4</sub>O<sub>7</sub> phase during oxidation reactions in the absence of HCl, which is again reducible (Figs. 5a, S4a and b) and thus causes the formation of CO<sub>x</sub>. The limited yield of chlorinated products formed on PrOCl (Fig. 1) is explained by its inability to release chlorine as seen from its negligible activity in HCl oxidation tests (Fig. 7c). In stark contrast to the above-mentioned systems, EuOCl-p-973 is essentially inactive for the C<sub>2</sub>H<sub>4</sub> and CO oxidation reactions (Fig. 7a and b), preserves the EuOCl phase under oxidizing conditions (Fig. S4), and has moderate ability to transfer chlorine as evidenced by its mild HCl oxidation activity above 673 K (Fig. 7c). Thus, it appears that the stability of the oxychloride phase and the ability to release chlorine from the surface are key to suppressing the formation of undesired oxidation products and to chlorinate ethylene.

Finally, the dehydrochlorination of EDC to VCM, was investigated by feeding 1.5 vol.% EDC without or with addition of 3 vol.% O<sub>2</sub> and 4.8 vol.% HCl to the feed (Fig. 7d). The EDC concentration was selected to simulate a 50% ethylene conversion to EDC. Furthermore, since CeO<sub>2</sub> was known to yield a 90% conversion to VCM in mixed EDC:O<sub>2</sub>:HCl feeds [13], a high EDC feed concentration was preferred to provide improved sensitivity to differences in the performance. Dehydrochlorination activity was observed in all cases. This differed from our previous study, in which CeO<sub>2</sub> was found to be inactive in a pure EDC feed. The latter finding can be explained by the fact that in the present study, we evaluated the dehydrochlorination performance on catalysts equilibrated in ethylene oxychlorination, which increased the acidity of these samples. Albeit demonstrating a limited selectivity to chlorinated products in ethylene oxychlorination, PrOCl displays the best

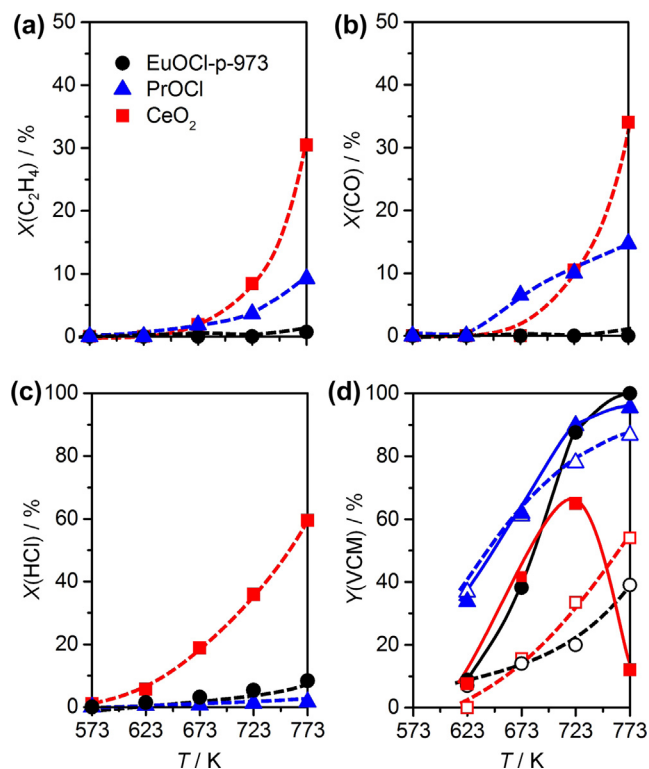


**Fig. 7.** Performance descriptors for selective VCM production over equilibrated catalysts. (a) C<sub>2</sub>H<sub>4</sub> oxidation to CO<sub>2</sub> (C<sub>2</sub>H<sub>4</sub>:O<sub>2</sub>:Ar:He = 3:3:3:91,  $W_{\text{cat}}/\dot{n}^0(\text{C}_2\text{H}_4) = 63 \text{ g h mol}^{-1}$ ), (b) CO oxidation to CO<sub>2</sub> (CO:O<sub>2</sub>:Ar:He = 2.5:2.5:3:92,  $W_{\text{cat}}/\dot{n}^0(\text{CO}) = 76 \text{ g h mol}^{-1}$ ), (c) HCl oxidation to Cl<sub>2</sub> (HCl:O<sub>2</sub>:Ar:He = 3:3:3:91,  $W_{\text{cat}}/\dot{n}^0(\text{HCl}) = 63 \text{ g h mol}^{-1}$ ), and (d) EDC dehydrochlorination to VCM. In (d)  $W_{\text{cat}}/\dot{n}^0(\text{EDC}) = 126 \text{ g h mol}^{-1}$ , open symbols: EDC: Ar:He = 1.5:3:95.5, and solid symbols: EDC: HCl:O<sub>2</sub>:Ar:He = 1.5:4.8:3:3:87.7.

EDC dehydrochlorination performance, with or without cofeeding oxygen and HCl, which can be linked to the highest density of acid sites evidenced in this material. However, the inferior performance of PrOCl in ethylene oxychlorination can be related to the low tendency of this catalyst to release chloride and its negligible reducibility (*vide supra*). CeO<sub>2</sub> demonstrates a linear dehydrochlorination trend with temperature when only EDC is fed, while an increased VCM yield and a shift to lower temperatures are attained when O<sub>2</sub> and HCl are mixed with the EDC. Nevertheless, at 773 K the yield is heavily decreased due to more extensive CO formation, which can be traced back to the higher reducibility of CeO<sub>2</sub> (Figs. 5a, 7a and b) that causes the combustion of chlorinated products. EuOCl-p-973 exhibits a linear trend with no CO<sub>x</sub> formation and an enhanced selectivity to VCM when HCl + O<sub>2</sub> is added to the feed.

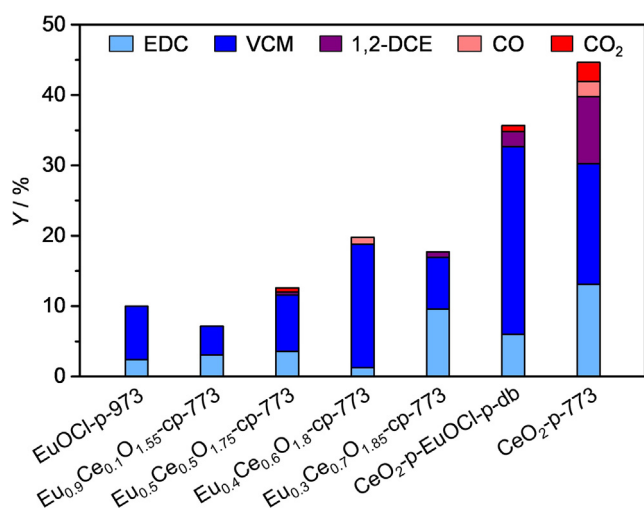
### 3.4. Integration of high activity and selectivity functions

The fact that the VCM yield over EuOCl is limited by its low intrinsic oxychlorination activity while the VCM selectivity over CeO<sub>2</sub> is compromised by the formation of CO<sub>x</sub> and over-chlorinated compounds, encouraged us to consider the possibility of integrating the advantageous qualities of each of these rare-earth compounds in the form of mixed oxides. Consequently, we prepared samples with molar fractions of europium ranging from 0.3 to 0.9 by coprecipitation (Table 2). The resulting materials were evaluated in ethylene oxychlorination at 673 K to maximize the activity while minimizing the likelihood of over-oxidation (Fig. 8). The yield of chlorinated products (and thus the C<sub>2</sub>H<sub>4</sub> conversion) is found to reach a maximum over Eu<sub>0.4</sub>Ce<sub>0.6</sub>O<sub>1.8</sub>-cp-773. A

**Table 2**

Characterization data and rate of VCM formation of the mixed europium-cerium oxides.

Sample	Eu:Ce <sup>a</sup> (mol mol <sup>-1</sup> )	S <sub>BET</sub> <sup>b</sup> (m <sup>2</sup> g <sup>-1</sup> )	r(VCM) <sup>c</sup> (mol h <sup>-1</sup> m <sup>-2</sup> )
Eu <sub>2</sub> O <sub>3</sub> -p-973	1:0	31	8.96 × 10 <sup>-6</sup>
Eu <sub>0.9</sub> Ce <sub>0.1</sub> O <sub>1.55</sub> -cp-773	0.9:0.1	16	9.25 × 10 <sup>-6</sup>
Eu <sub>0.5</sub> Ce <sub>0.5</sub> O <sub>1.75</sub> -cp-773	0.51:0.49	13	2.24 × 10 <sup>-5</sup>
Eu <sub>0.4</sub> Ce <sub>0.6</sub> O <sub>1.8</sub> -cp-773	0.39:0.61	27	2.36 × 10 <sup>-5</sup>
Eu <sub>0.3</sub> Ce <sub>0.7</sub> O <sub>1.85</sub> -cp-773	0.3:0.7	25	1.07 × 10 <sup>-5</sup>
CeO <sub>2</sub> -p-773	0:1	44	1.41 × 10 <sup>-5</sup>
CeO <sub>2</sub> -p-EuOCl-p-db	0.4:0.6 <sup>d</sup>	39 <sup>d</sup>	2.49 × 10 <sup>-5</sup>

<sup>a</sup> XRF.<sup>b</sup> BET method.<sup>c</sup> Corresponds to data in Fig. 8.<sup>d</sup> Estimated.**Fig. 8.** Product yields in ethylene oxychlorination over EuOCl-p-973, CeO<sub>2</sub>-p-773, mixed oxides of Eu and Ce, and the dual-bed configuration of CeO<sub>2</sub>-p-773 and EuOCl-p-973. Conditions:  $T = 673$  K,  $C_2H_4:HCl:O_2:Ar:He = 3:4.8:3:3:86.2$ ,  $W_{cat}/\dot{n}^0(C_2H_4) = 63$  g h mol<sup>-1</sup>.

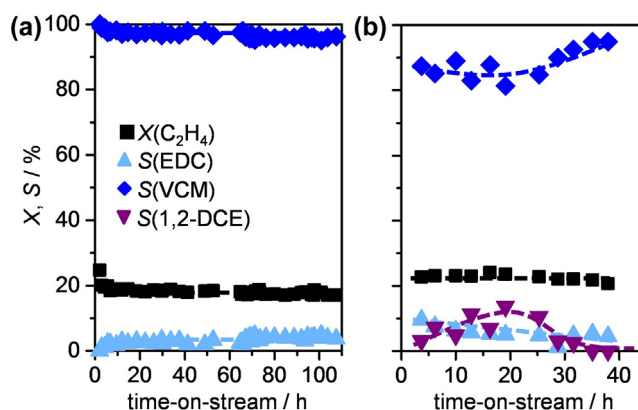
further increase in cerium contents in these precipitated samples causes a drop in activity and also leads to the formation of over-chlorinated products (1,2-DCE).

Analysis by N<sub>2</sub> sorption indicated that the total surface area of the mixed oxides was generally lower than the corresponding single phases (Table 2), which gives a first hint of the interaction of Eu and Ce in these systems. Due to the similar crystal structures of Eu<sub>2</sub>O<sub>3</sub> and CeO<sub>2</sub>, it is difficult to conclude whether the fresh Eu<sub>x</sub>-Ce<sub>1-x</sub>O<sub>2-0.5x</sub>-cp- $T_{cal}$  materials are physical mixtures of the single oxides or atomically-dispersed mixed metal oxides (i.e., having metal to metal interactions/bonding within the oxide network) by XRD (Fig. S5). Analysis of the equilibrated samples only evidences the presence of the EuOCl phase in samples with a europium fraction above 0.6. The fact that the oxychloride is not observed for  $x \leq 0.5$  corroborates the strong interaction between Eu and Ce in the mixed phase. Consistently, the cell parameter of 5.38 Å was derived for Eu<sub>0.4</sub>Ce<sub>0.6</sub>O<sub>1.8</sub>-cp-773, the best sample in terms of VCM yield, which lies between that of the CeO<sub>2</sub>-p-773 (5.35 Å) and Eu<sub>2</sub>O<sub>3</sub>-p-773 (5.41 Å). Examination by electron microscopy (Fig. 3e) shows that the equilibrated sample is composed of small nanoparticles of ca. 5–10 nm, preserving the crystallinity of the as prepared material (not shown for brevity). The elemental map reveals a very homogeneous distribution of europium and cerium atoms, which is also similar to the fresh analogue. Interestingly, the EDX spectrum evidences a small amount of chlorine in the equilibrated sample, which is also corroborated by XPS results showing a shift of the Eu 4d<sub>3/2</sub> and Eu 4d<sub>5/2</sub> peaks to higher binding

energy compared to the as-prepared sample due to the presence of chlorine (Fig. 4b). Thus, the oxychloride phase could still exist at the surface leading to high acidity. This reasoning is consistent with the highest VCM yield of this sample (Fig. 1). Comparing the performance of Eu<sub>0.4</sub>Ce<sub>0.6</sub>O<sub>1.8</sub>-cp-773 with EuOCl-p-973 and CeO<sub>2</sub>-p-773, it is clear that the mixed oxide leads to very selective VCM formation (Fig. 8) and minimal combustion.

Since stability is a crucial driver in the hunt for new catalytic systems to improve the current ethylene oxychlorination process, the long-term performance of EuOCl-p-973 and Eu<sub>0.4</sub>Ce<sub>0.6</sub>O<sub>1.8</sub>-cp-773 was evaluated, demonstrating a stable operation in ethylene oxychlorination for over 100 h and 40 h on stream with VCM yields of 15% and 19%, respectively (Fig. 9). Even though a minor amount of 1,2-DCE (estimated by carbon mass balance error of about 5–6%) is observed for Eu<sub>0.4</sub>Ce<sub>0.6</sub>O<sub>1.8</sub>-cp-773 up to 20 h, after which it drops with time-on-stream, the mixed oxide evidences higher activity as it is operated at 50 K lower temperature and one-fourth of the space time (63 g h mol<sup>-1</sup> compared to 252 g h mol<sup>-1</sup>). To further assess the stability of EuOCl, we conducted a catalytic test doubling the reactant concentration, which resulted in a very similar selectivity pattern (4% EDC, 96% VCM) as observed under standard conditions at comparable C<sub>2</sub>H<sub>4</sub> conversion (19%). Besides, no volatilization of the active phase was evidenced, for example by deposits commonly observed on the reactor walls when using unstable materials, under either condition. Still, the VCM yield achieved is not yet optimal (Fig. 8). In fact, although CeO<sub>2</sub>-p-773 suffers from CO<sub>x</sub> and 1,2-DCE formation, the overall yield of desired EDC and VCM was higher compared to Eu<sub>0.4</sub>Ce<sub>0.6</sub>O<sub>1.8</sub>-cp-773.

As an alternative approach to improve the VCM yield, CeO<sub>2</sub> and EuOCl were united in a dual-bed reactor, combining the high

**Fig. 9.** C<sub>2</sub>H<sub>4</sub> conversion and product selectivities versus time-on-stream in ethylene oxychlorination over (a) EuOCl-p-973 and (b) Eu<sub>0.4</sub>Ce<sub>0.6</sub>O<sub>1.8</sub>-cp-773. Conditions:  $T = 723$  K (673 K for Eu<sub>0.4</sub>Ce<sub>0.6</sub>O<sub>1.8</sub>-cp-773),  $C_2H_4:HCl:O_2:Ar:He = 3:4.8:1.5:3:87.7$  ( $C_2H_4:HCl:O_2:Ar:He = 3:4.8:3:3:86.2$  for Eu<sub>0.4</sub>Ce<sub>0.6</sub>O<sub>1.8</sub>-cp-773),  $W_{cat}/\dot{n}^0(C_2H_4) = 252$  g h mol<sup>-1</sup> (63 g h mol<sup>-1</sup> for Eu<sub>0.4</sub>Ce<sub>0.6</sub>O<sub>1.8</sub>-cp-773).

activity of CeO<sub>2</sub> in a first bed in the direction of flow in order to enhance the EDC formation with the unique selectivity to VCM of EuOCl due to its acidity in a second bed (CeO<sub>2</sub>-p-EuOCl-p-db). Advantageously, this could also enable an efficient utilization of the heat generated by the exothermic oxychlorination in the downstream endothermic dehydrochlorination. This system indeed results in the highest VCM (27%) and VCM + EDC (33%) yields observed so far at the standard space time of 63 g h mol<sup>-1</sup> applied in this study. Even though small amounts of side products (CO<sub>2</sub> and 1,2-DCE) are formed in the first bed by CeO<sub>2</sub> (Fig. 8), this dual-bed system shows the highest rate of VCM production per unit surface area of the catalyst (Table 2). Since both, EuOCl (Fig. 9) and CeO<sub>2</sub> [13] are individually stable, a highly robust operation of this dual-bed reactor can be anticipated.

#### 4. Conclusions

In this study, we developed a fundamental understanding of the ethylene oxychlorination chemistry on scarcely studied rare-earth compounds. Through the integration of steady-state catalytic tests and advanced characterization, we identified EuOCl as the best catalyst for direct VCM production, leading to 96% selectivity and no CO<sub>x</sub> formation at 20% ethylene conversion for over 100 h on stream. The consecutive conversion of ethylene to EDC and EDC to VCM confirmed the bifunctional reaction mechanism over this catalyst. This unique behavior was found to originate from the transformation of the initial Eu<sub>2</sub>O<sub>3</sub> phase to a stable oxychloride. The latter was completely inert toward ethylene and CO oxidation, which explains the absence of undesired CO<sub>x</sub>, while it exhibited moderate HCl oxidation, demonstrating its ability to chlorinate ethylene. Other lanthanide oxides, except CeO<sub>2</sub> which retained the oxide structure after reaction, also transformed to their respective oxychloride or chloride phases. However, these oxychlorides were either essentially inactive in ethylene oxychlorination or decomposed in oxidative conditions and catalyzed undesired oxidations forming significant amounts of CO<sub>x</sub>, as demonstrated for the case of PrOCl. Another crucial aspect of the EuOCl phase was the presence of a high concentration of acid sites, which catalyzed the EDC dehydrochlorination to produce VCM. By combining CeO<sub>2</sub> for its high activity toward EDC with Eu<sub>2</sub>O<sub>3</sub> or EuOCl for VCM, in the form of homogeneously mixed oxides or as a dual-bed system, respectively, we demonstrated industrially attractive VCM yields (ca. 30%). The intensification feasibility studied herein can be anticipated to be more economical than the current two-step process as it enables reduction of the unit operations eliminating the need for the intermediate EDC purification and subsequent cracking steps.

#### Acknowledgments

This work was sponsored by the Swiss National Science Foundation (Project No. 200021-156107). The authors acknowledge Dr. R. Hauert (Empa, Switzerland) for XPS analysis.

#### Appendix A. Supplementary material

Supplementary data associated with this article can be found, in the online version, at <http://dx.doi.org/10.1016/j.jcat.2016.10.026>.

#### References

- [1] Renolit, Everything about PVC, 2015. <[http://www.renolit.com/fileadmin/renolit/corporate/images/Everything\\_about\\_PVC.pdf](http://www.renolit.com/fileadmin/renolit/corporate/images/Everything_about_PVC.pdf)> (accessed July 22, 2016).
- [2] Plastics Today, Global PVC Demand to grow 3.2% Annually through 2021, 2014. <<http://www.plasticstoday.com/study-global-pvc-demand-grow-32-annually-through-2021/196257501821043>> (accessed July 22, 2016).
- [3] K. Weissmehl, H.-J. Arpe, Industrial Organic Chemistry, Wiley-VCH, Weinheim, 2008, pp. 217–224.
- [4] E.-L. Dreher, K.K. Beutel, J.D. Myers, T. Lübke, S. Krieger, L.H. Pottenger, Ullmann's Encyclopedia of Industrial Chemistry, Wiley-VCH, Weinheim, 2000, pp. 9–17.
- [5] J.S. Naworski, E.S. Velez, Applied Industrial Catalysis, Academic Press, New York, 1983, p. 239.
- [6] N.B. Muddada, U. Olsbye, L. Caccialupi, F. Cavani, G. Leofanti, D. Gianolio, S. Bordiga, C. Lamberti, Influence of additives in defining the active phase of the ethylene oxychlorination catalyst, *Phys. Chem. Chem. Phys.* 12 (2010) 5605–5618.
- [7] N.B. Muddada, T. Fuglerud, C. Lamberti, U. Olsbye, Tuning the activity and selectivity of CuCl<sub>2</sub>/γ-Al<sub>2</sub>O<sub>3</sub> ethene oxychlorination catalyst by selective promotion, *Top. Catal.* 57 (2014) 741–756.
- [8] F.E. Van Rooijen, A. De Bruijn, J. Johan, Catalytic Oxychlorination, US Patent US2009/0054708 A1, to Albemarle Netherlands B.V., 2009.
- [9] M. Valentacchi, C. Rubini, Oxychlorination Catalytic Composition for Controlling Exothermic Reactions in a Fixed Bed, European Patent 1 020 222 B1, to Süd Chemie Mt S.R.L., 2004.
- [10] I.M. Clegg, R. Hardman, Vinyl Chloride Production Process, US Patent 5 728 905, to EVC Technologies AG, 1998.
- [11] L.J. Croce, L. Bajars, M. Gabliks, Oxychlorination of Hydrocarbons in the Presence of Non-Halide Copper containing Catalysts, US Patent 4 025 461, to Petro-Tex Chemical Corporation, 1977.
- [12] M.E. Jones, M.M. Olken, D.A. Hickman, Process for the Conversion of Ethylene to Vinyl Chloride and Novel Catalyst Compositions Useful for Such Process, US Patent 6 909 024 B1, to The Dow Chemical Company, 2005.
- [13] M. Scharfe, P.A. Lira-Parada, V. Paunović, M. Moser, A.P. Amrute, J. Pérez-Ramírez, Oxychlorination-dehydrochlorination chemistry on bifunctional ceria catalysts for intensified vinyl chloride production, *Angew. Chem. Int. Ed.* 55 (2016) 3068–3072.
- [14] M.A. Centeno, P. Malet, I. Carrizosa, J.A. Odriozola, Lanthanide doped V<sub>2</sub>O<sub>5</sub>/Al<sub>2</sub>O<sub>3</sub> catalysts: structure-activity relationship in the SCR of NO<sub>x</sub>, *J. Phys. Chem. B* 104 (2000) 3310–3319.
- [15] W.Y. Hernández, F. Romero-Sarria, M.A. Centeno, J.A. Odriozola, In situ characterization of the dynamic gold-support interaction over ceria modified Eu<sup>3+</sup>. Influence of the oxygen vacancies on the CO oxidation reaction, *J. Phys. Chem. C* 114 (2010) 10857–10865.
- [16] T. Montini, M. Melchionna, M. Monai, P. Fornasiero, Fundamentals and catalytic applications of CeO<sub>2</sub>-based materials, *Chem. Rev.* 116 (2016) 5987–6041.
- [17] M. Cargnello, N.L. Wieder, T. Montini, R.J. Gorte, P. Fornasiero, Synthesis of dispersible Pd@CeO<sub>2</sub> core-shell nanostructures by self-assembly, *J. Am. Chem. Soc.* 132 (2010) 1402–1409.
- [18] K. Tamm, R. Kungas, R.J. Gorte, E. Lust, Solid oxide fuel cell anodes prepared by infiltration of strontium doped lanthanum vanadate into doped ceria electrolyte, *Electrochim. Acta* 106 (2013) 398–405.
- [19] J. Kašpar, P. Fornasiero, M. Graziani, Use of CeO<sub>2</sub>-based oxides in the three-way catalysis, *Catal. Today* 50 (1999) 285–298.
- [20] D. Valechha, S. Lokhande, M. Klementova, J. Subrt, S. Rayalu, N.L. Labhsetwar, Study of nano-structured ceria for catalytic CO oxidation, *Mater. Chem.* 21 (2011) 3718–3725.
- [21] C. de Leitenburg, A. Trovarelli, J. Llorca, F. Cavani, G. Bini, The effect of doping CeO<sub>2</sub> with zirconium in the oxidation of isobutene, *Appl. Catal. A* 139 (1996) 161–173.
- [22] A.P. Amrute, C. Mondelli, M. Moser, G. Novelli-Leruth, N. López, D. Rosenthal, R. Farra, M.E. Schuster, D. Teschner, T. Schmidt, J. Pérez-Ramírez, Performance, structure, and mechanism of CeO<sub>2</sub> in HCl oxidation to Cl<sub>2</sub>, *J. Catal.* 286 (2012) 287–297.
- [23] M. Moser, A.P. Amrute, J. Pérez-Ramírez, Impact of feed impurities on catalysts for chlorine recycling, *Appl. Catal. B* 162 (2015) 602–609.
- [24] J.H. Lunsford, The catalytic oxidative coupling of methane, *Angew. Chem. Int. Ed.* 34 (1995) 970–980.
- [25] T.J. Toops, A.B. Walters, M.A. Vannice, The effect of CO<sub>2</sub> and H<sub>2</sub>O on the kinetics of NO reduction by CH<sub>4</sub> over a La<sub>2</sub>O<sub>3</sub>/γ-Al<sub>2</sub>O<sub>3</sub> catalyst, *J. Catal.* 214 (2003) 292–307.
- [26] S.G. Podkolzin, E.E. Stangland, M.E. Jones, E. Peringer, J.A. Lercher, Methyl chloride production from methane over lanthanum-based catalysts, *J. Am. Chem. Soc.* 129 (2007) 2569–2576.
- [27] J. He, T. Xu, Z. Wang, Q. Zhang, W. Deng, Y. Wang, Transformation of methane to propylene: a two-step reaction route catalyzed by modified CeO<sub>2</sub> nanocrystals and zeolites, *Angew. Chem. Int. Ed.* 51 (2012) 2438–2442.
- [28] S. Brunauer, P.H. Emmett, E. Teller, Adsorption of gases in multimolecular layers, *J. Am. Chem. Soc.* 60 (1938) 309–319.
- [29] F. Mercier, C. Alliot, L. Bion, N. Thomat, P. Toulhoat, XPS study of Eu(III) coordination compounds: Core levels binding energies in solid mixed-oxo-compounds Eu<sub>m</sub>X<sub>n</sub>O<sub>y</sub>, *J. Electron. Spectrosc. Relat.: Phenom.* 150 (2006) 21–26.
- [30] S. Kumar, R. Prakash, R.J. Choudhary, D.M. Phase, Structural, XPS and magnetic studies of pulsed laser deposited Fe doped Eu<sub>2</sub>O<sub>3</sub> thin film, *Mater. Res. Bull.* 70 (2015) 392–396.
- [31] Y. Uwamino, A. Tsuge, T. Ishizuka, H. Yamatera, X-ray photoelectron spectroscopy of rare earth halides, *Bull. Chem. Soc. Jpn.* 59 (1986) 2263–2267.
- [32] A.S. Shalygin, L.V. Malysheva, E.A. Paukshtis, Mechanism of 1,2-dichloroethane dehydrochlorination on the acid sites of oxide catalysts as studied by IR spectroscopy, *Kinet. Catal.* 52 (2011) 305–315.

- [33] H.C. Yao, Y.F. Yu Yao, Ceria in automotive exhaust catalysts: I. Oxygen storage, *J. Catal.* 86 (1984) 254–265.
- [34] A. Trovarelli, Catalytic properties of ceria and CeO<sub>2</sub>-containing materials, *Catal. Rev. -Sci. Eng.* 38 (1996) 439–518.
- [35] R. Farra, S. Wrabetz, M.E. Schuster, E. Stotz, N.G. Hamilton, A.P. Amrute, J. Pérez-Ramírez, N. López, D. Teschner, Understanding CeO<sub>2</sub> as a deacon catalyst by probe molecule adsorption and *in situ* infrared characterizations, *Phys. Chem. Chem. Phys.* 15 (2013) 3454–3465.